Spin waves of a current-injected thin ferromagnetic stripe

R. P. Erickson* and D. P. Pappas
National Institute of Standards and Technology, Boulder, Colorado 80305, USA
(Received 4 August 2008; revised manuscript received 24 September 2008; published 27 October 2008)

Within a micromagnetic model we present the theory of linearized spin waves of a current-carrying rectangular ferromagnetic stripe treated as a slab of infinite extent. After determining the nonuniform scissorlike magnetic ground state that results when a dc electric current is applied along an in-plane easy axis, we calculate both ferromagnetic resonances and spin-wave dispersion as a function of slab thickness. For Permalloy stripes less than 1 μm in thickness, increasing current stiffens the response of bulk spin waves, and their dispersion becomes increasingly asymmetric with respect to the easy axis—shifting to lower (higher) frequencies with (opposite) the direction of current. Also, the frequency and direction of propagation of the Damon-Eshbach surface mode are substantially modified by the current, with changed surface-mode behavior exhibited. Above 1 μm in thickness the lowest-lying resonance frequency of the Permalloy stripe softens to zero with increasing current and a gap opens up to finite wavelengths along the direction of current, indicative of a ground-state instability. We discuss the implication of our results to the characterization of the magnetic state of these rectangular structures.

DOI: 10.1103/PhysRevB.78.144421 PACS number(s): 75.30.Ds, 75.25.+z, 76.50.+g

I. INTRODUCTION

Fabrication of nanoscale materials that couple electron charge to spin quanta, so-called spintronic or magnetoelectronic devices, has created a burgeoning field of study in the last couple of decades,[1] elicited by the discovery of giant magnetoresistance (GMR) in Fe/Cr/Fe multilayers.[2] Most notably, the spin-valve device, which exploits the GMR effect, has gained widespread use in read-write heads within the magnetic recording industry. More recently, experiments involving the injection of spin-polarized current into magnetic nanopillars[3,4] have led to observations of coupled nonlinear magnetic oscillations of significant size within these structures.[5,6] In particular, Pufall *et al.*,[4] in their elegant experiment, suggested that the interaction of their nano-oscillators is mediated by spin waves. Recent theoretical studies of spin waves in the presence of a transport current have focused on the disk shape.[7,8] Other theoretical studies of spin waves in cylindrical ferromagnetic nanowires have also been discussed in the presence of both Zeeman[9] and microwave[10] fields.

As demonstrated in Ref. 4, pulses of electric current applied at frequencies in the gigahertz range can induce spin waves in ferromagnetic structures. In the present paper we consider unpolarized current pulses of frequencies orders of magnitude lower, where the temporal width of the pulse is of sufficient duration that one may model the current by its dc component and corresponding Oersted field. In this limit a well-defined magnetic ground state can be sustained for the duration of the pulse, and excitations of this ground state are spin waves generated by means other than the current itself.

While there is a long history of theoretical descriptions of micromagnetic order and spin waves in rectangular, cylindrical, and spherical geometries, as far as we know a thorough account of spin-wave excitations of the ferromagnetic slab in the presence of a transport current, as we envisage here, has not been presented in the literature. Some years ago, Smith *et al.*[11] presented a micromagnetic theory of ferromagnetic order in current-carrying thin films, with application to Permalloy stripes possessing an in-plane easy axis of magnetization, associated with volume anisotropy of strain-induced origin. In this situation, the application of current along the easy axis causes the magnetization to spread out in either direction, away from the easy axis, in an arrangement that can be described as a scissor configuration. This fanlike arrangement is a consequence of the fact that the applied current induces an Oersted field in plane and perpendicular to the easy axis but in opposite directions with respect to the top and bottom of the slab. The Oersted field increases linearly in magnitude from zero, at the center of the slab, to a maximum value at the slab surfaces. The success of Ref. 11 was to show how the model exchange constant could be accurately quantified by fitting to magnetoresistive measurements obtained while current was applied along the easy axis.

In the present paper we expand on the work in Ref. 11 by providing an account of the linearized spin-wave excitation spectrum of the nonuniform classical magnetic ground state that arises in this rectangular geometry—with an unpolarized dc electric current applied along the in-plane easy axis. As in Ref. 11, we have in mind rectangular Permalloy stripes where the width perpendicular to the easy axis is much greater than the thickness of the stripe, such that we can approximate the stripe as a ferromagnetic slab with top and bottom surfaces of infinite extent. A classical theory of spin waves established within a micromagnetic model of these structures permits their characterization through such experimental techniques as ferromagnetic resonance (FMR) and Brillouin light scattering (BLS).[12] Additionally, it allows us to investigate the stability of the scissorlike ground state under such forms of magnetic excitation as these experimental techniques induce.

Our model assumes a spatial continuum wherein exchange enters through the gradient of magnetization. Thus,

our model is lacking in that it only addresses the long-wavelength limit of exchange interaction. Hence, it cannot describe the exchange-dominated surface spin waves of the rectangular geometry, which are prominent at the Brillouin-zone edge, as might be calculated from a spin Hamiltonian of the discrete lattice.[13] Also, by assuming surfaces of infinite extent we neglect the effects of domain-wall formation at stripe edges, as might be important in stripes of narrow cross section. Nevertheless, we are able to determine in detail how the transport current applied to wide stripes modifies spin-wave states of the long-wavelength regime wherein both dipolar fields and exchange act. We accomplish this through an exact numerical treatment of the dipolar field of the film geometry, which allows us to calculate spin-wave excitations for a large range of stripe thicknesses and highly nonuniform ground-state configurations. In very thin stripes we show how the transport current stiffens the frequency response of bulk spin-wave modes and how the current affects the evolution and propagation of the Damon-Eshbach surface mode[14] as this mode forms with increasing thickness. For thicker stripes we find that increasing the applied current eventually leads to a gap developing in the spin-wave dispersion of the lowest-lying band, along the direction of current, extending from the point of resonance to finite wavelengths, indicative of an unstable scissorlike magnetic ground state.

In the magnetic ground state section we discuss the model and calculations of the classical ground-state magnetic order that arises from it. In the spin wave analyses section, we present the theory of spin-wave excitations of the magnetic scissor state, solving the linearized Landau-Lifshitz equations of motion in the presence of a transport current. We then discuss calculations of spin-wave modes of the scissorlike ground state. In the concluding remarks section, we comment on our results and their application to ongoing research.

II. MAGNETIC GROUND STATE

A. Model of the current-carrying ferromagnetic stripe

We consider a rectangular stripe in the form of a thin slab with parallel surfaces of area S separated by a distance d, where either dimension of S is much greater than d, such that for all intents and purposes the stripe can be viewed as infinite in extent. As depicted in Fig. 1, with respect to Cartesian coordinates x, y, and z, let the two surfaces represent infinite planes in x-y at positions $z=\pm z_0$, such that the stripe thickness is $d=2z_0$. The stripe is ferromagnetic (when no current is applied), such that a uniform arrangement of magnetization with saturation magnitude M_0 is established everywhere within the stripe by an isotropic exchange constant A. Also, uniaxial magnetoelastic anisotropy exists throughout the volume of the stripe, with easy axis in the x direction, assumed induced with growth, via strain, in conjunction with a Zeeman field of magnitude H_{Zeeman} applied along the positive x axis. Consequently the uniformly magnetized state lies along the positive x direction in the plane of the stripe.

If a transport current density J is introduced along the positive x axis, as in the figure, then the magnetization can be modeled as $\vec{M}(z)=M_0 \cos\theta(z)\hat{x}+M_0 \sin\theta(z)\hat{y}$, which has

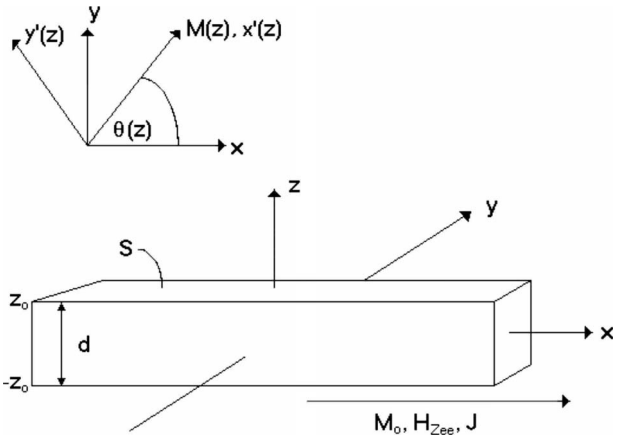

FIG. 1. Diagram depicting the orientation of magnetization $M(z)$, of saturation value M_0, within an infinite ferromagnetic slab of thickness $d=2z_0$ (center at $z=0$) and surfaces of area S. The Zeeman field H_{Zeeman} and electric current density J are applied along the easy axis x, as indicated. The coordinate axes $x'(z)$ and $y'(z)$ are rotated by angle $\theta(z)$, which is a negative (positive) angle for values of $z>0$ ($z<0$).

zero divergence everywhere. By symmetry, we require the angle $\theta(z)$ to be such that $\theta(-z)=-\theta(z)$, which implies $\theta(0)=0$. The current density J induces an Oersted magnetic field within the stripe, which by Ampere's law can written as

$$\vec{H}(z)=H_J(z)\hat{y}, \quad H_J(z)=-\frac{4\pi}{c}Jz. \tag{1}$$

The Oersted field is continuous across the surfaces S and is of constant magnitude outside the stripe, where it is equal to the magnetic induction. Its effect within the stripe is to partially demagnetize the uniform state of the stripe, leading to the scissorlike magnetic state described by angle $\theta(z)$, where z is the distance from the center of the stripe. Note that within the top portion of the stripe the Oersted field is aligned with the $-y$ direction, such that the tendency of magnetization to align in this field implies $\theta(z)<0$ when $z>0$.

Our model of the rectangular geometry does not include surface anisotropy. Most of our calculations are for stripe thicknesses greater than a few tens of angstroms, so we expect surface anisotropy to play a minor role in comparison with exchange and the Oersted field. Furthermore, Smith *et al.*,[11] in their studies of slabs that were thousands of angstroms thick, determined that best fits to magnetoresistance data were achieved when surface anisotropy was ignored.

In order for the magnetic scissor state to be observable it must at least be energetically more favorable than the uniform state. To make this comparison we construct the Gibbs free energy.[15] With magnetization $\vec{M}(\vec{x})$ and magnetic field $\vec{H}(\vec{x})$, as given by Eq. (1), the free energy is the sum of four parts, whose energy densities can be written as (i) $A|\nabla\hat{M}(\vec{x})|^2$, an exchange term ($A>0$), (ii) $-K\cdot\hat{M}_x(\vec{x})^2$, a uniaxial volume anisotropy term with easy axis x($K>0$), (iii) $-\vec{M}(\vec{x})\cdot\vec{H}(\vec{x})$, an Oersted interaction term, and (iv) $-M(\vec{x})\cdot\vec{H}_{\text{Zeeman}}$, a Zeeman term. Summing these contribu-

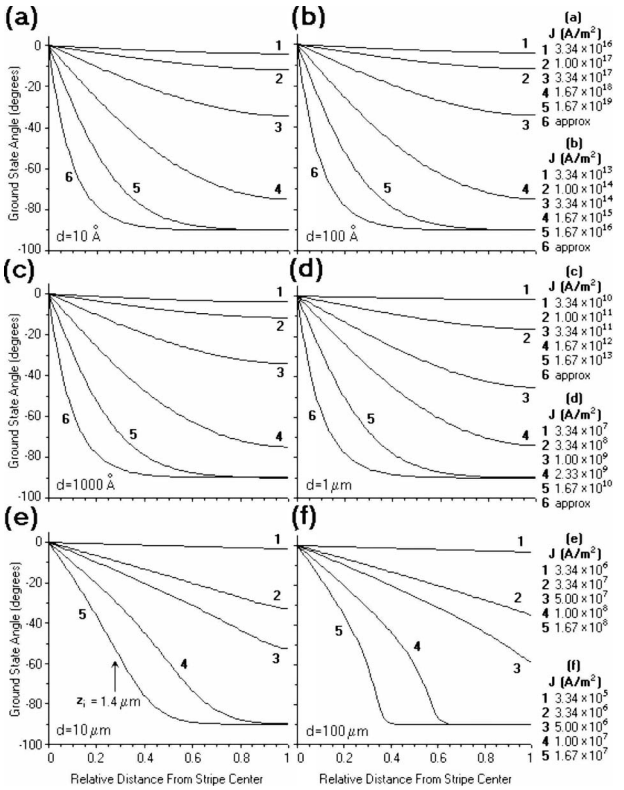

FIG. 2. Angle of ground-state magnetization (from easy axis) in upper half of the stripe, as a function of relative distance from center, for increasing values of current density J and thickness d. Results are determined numerically from Eq. (3) except the curves labeled 6, which are plots of Eq. (4b); curves 6 correspond to the same value of J as curves 5. At (e) there is a change in inflection of angular profile z_i as the magnetization tends toward saturation in the Oersted field. This is due to the relative weakness of the Oersted field within the bulk of the stripe as d increases.

tions over the volume of the stripe and applying symmetry, the Gibbs free energy of the magnetic scissor state is

$$G[\theta(z)] = 2S\int_0^{z_0} \{A\dot{\theta}(z)^2 + K\sin^2\theta(z) - M_0H_J(z)\sin\theta(z) + M_0H_{\text{Zeeman}}[1-\cos\theta(z)]\}\cdot dz, \tag{2}$$

where $\dot{\theta}(z) \equiv d\theta(z)/dz$ and, in a last step, we have subtracted from the energy the contribution of the uniformly magnetized state, where $\theta(z) \equiv 0$ for all $|z| < z_0$, such that $G[0] \equiv 0$.

Now Eq. (2) is a functional of $\theta(z)$, with integrand explicitly a function of θ, $\dot{\theta}$, and z. If we minimize Eq. (2) to find the ground-state angle $\theta(z)$, where we hold the end point $z=0$ fixed [because $\theta(0)=0$] and allow the end point $z=z_0$ to vary freely (because it has no *a priori* constraint), then we obtain two conditions. One is the usual Euler-Lagrange equation, which we may express as

$$\frac{2A}{M_0}\ddot{\theta}(z) - \frac{K}{M_0}\sin 2\theta(z) + H_J(z)\cos\theta(z) - H_{\text{Zeeman}}\sin\theta(z) = 0. \tag{3a}$$

The other, stemming from the allowance for a free end point $z=z_0$, states that the derivative of $\theta(z)$ with respect to z must vanish at the surfaces. Hence, along with the symmetry condition $\theta(0)=0$, we have two boundary conditions,

$$\theta(0) = 0, \quad \dot{\theta}(z_0) = 0, \tag{3b}$$

which Eq. (3a) must satisfy. Taken together, Eqs. (3a) and (3b) define the classical magnetic ground state in the presence of the transport current, in the upper half of the stripe, where $0 < z < z_0$. The solution of $\theta(z)$ in the bottom half of the stripe, where $-z_0 < z < 0$, is obtained from $\theta(-z) = -\theta(z)$.

B. Calculations of the magnetic ground state with applied current

We solved Eq. (3) via a numerical relaxation technique,[16] which involves inputting an initial guess for the $\theta(z)$ profile. This method works best if one starts from a known solution, such as the uniform state of zero applied current or an analytical approximation. For each solution we computed the free energy per area S using Eq. (2), via a simple trapezoidal summation, with relaxation calculations that employed 100 mesh points. This technique is fairly robust although convergence becomes more difficult as current density J is increased or as stripe thickness d increases. Figure 2 illustrates angular profiles of ground-state magnetization for a range of applied current densities and stripe thicknesses applicable to Permalloy stripes, where $A = 1.0\times10^{-6}$ cm^{-3}, $4\pi M_0 = 10\,020$ G, and $K = 1450$ erg/cm^3.

Equation (3a) is a nonlinear second-order differential equation that possesses multiple nonadditive solutions for a given set of input parameters. For example, with $H_{\text{Zeeman}} = 0$, Eq. (3a) emits constant solutions of the form $\theta(z) = \pi(2n+1)/2$, where n is an integer. These are, in fact, asymptotes for different sets of solutions, where the asymptotes characterize how the various solutions approach saturation in the Oersted field. In our numerical analyses we found magnetic ground-state solutions (with respect to the upper half of the stripe) to be a set monotonically asymptotic to the $n=-1$ case. For example, in Fig. 3(a) we show results for the free energy per surface area of the stripe, as calculated from Eq. (2), as a function of stripe thickness, for a range of current densities. Here, $G[\theta(z)]/S < 0$ indicates that the scissor ground state, which forms in the presence of the transport current, is of lower energy than the uniform state of magnetization and increasingly so with greater stripe thickness. Occasionally, particularly in high-Oersted fields, we found that the numerical relaxation algorithm converged to a solution that was either nonmonotonic, i.e., vortexlike, or not asymptotic to $\theta(z) = -\pi/2$, but we easily rejected such cases as ground states since their free energies were always higher than those both monotonic and asymptotic to the $\theta(z) = -\pi/2$ solution.

An analytical approximation of Eq. (3) can be realized by linearizing the differential equation with respect to $\theta(z)$. The result, previously described in the literature,[11] is

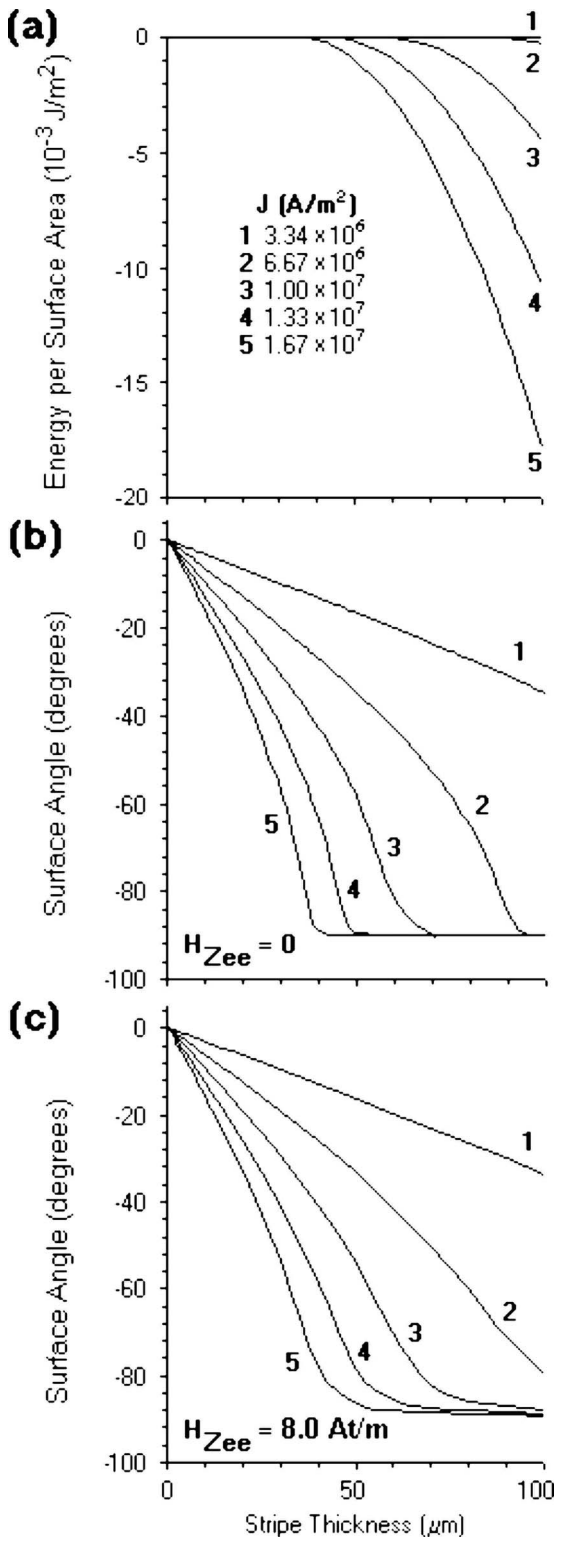

FIG. 3. Magnetic ground-state calculations as a function of thickness d for a range of labeled current densities J. In (a) the Gibbs free energy per surface area of the stripe as a function of thickness, illustrating stability of the magnetic scissor state compared to the uniformly magnetized state. In (b) the corresponding angle of the magnetization at the top surface of the stripe. In (c), as a contrast to the results depicted in (b), an external magnetic field H_{Zeeman} of 8.0 At/m is applied to illustrate the strength of rotation back to the easy axis.

$$\theta(z) \cong \frac{-4\pi M_0 J}{c(2K + M_0 H_{\mathrm{Zeeman}})}\left[z - \sqrt{\frac{2A}{2K + M_0 H_{\mathrm{Zeeman}}}} \times \frac{\sinh\left(z\sqrt{\frac{2K + M_0 H_{\mathrm{Zeeman}}}{2A}} \right)}{\cosh\left(z_0\sqrt{\frac{2K + M_0 H_{\mathrm{Zeeman}}}{2A}} \right)} \right]. \tag{4a}$$

However, this approximation is only valid in the limit of low-Oersted fields. In high-Oersted fields an alternative is to substitute $\theta(z) = -\pi/2 + \delta\theta(z)$ into Eq. (3a) and linearize with respect to $\delta\theta(z)$. In this instance we ignore the anisotropy term since we assume that in high-Oersted fields the ground state is more or less governed by the interplay between transport current and exchange at least for thin stripes. Also, we set the Oersted field of Eq. (1) to its value at z_0—the largest contribution of this term. This last step limits the accuracy of our approximation of $\theta(z)$ near the stripe center but provides a reasonable estimate of $\theta(z)$ near the surface. The approximation can be expressed as

$$\theta(z) \cong \left(-\frac{\pi}{2} + \frac{cH_{\mathrm{Zeeman}}}{4\pi J z_0} \right) \times \left\{ 1 - \frac{\cosh\left[(z_0 - z)\sqrt{\frac{2\pi M_0 J z_0}{cA}} \right]}{\cosh\left(z_0\sqrt{\frac{2\pi M_0 J z_0}{cA}} \right)} \right\}. \tag{4b}$$

The first four panels of Fig. 2, (a)–(d), include a plot of Eq. (4b) labeled as curve "6." Each curve 6 corresponds to a current density J equal to that of its respective neighboring curve "5." The asymptotic approach to saturation in the Oersted field depicted by each curve 6 goes as $\theta(z) \cong -(\pi/2)[1 - \exp(-z\sqrt{2\pi M_0 J z_0/cA})]$.

The alphabetic progression of panels in Fig. 2 illustrates the angular profile of the ground-state magnetization across the thickness of the stripe as this thickness increases from 10 Å to 100 μm. In panels (a)–(d) we see that as thickness is increased by 1 order of magnitude the current density required to achieve comparable scissorlike deflection of magnetization reduces by 3 orders of magnitude. This is evident from Eq. (4b), where the arguments of the cosh functions are proportional to three-halves the power of distance and one-half the power of current density. In 2(e), however, corresponding to a thickness of 10 μm, we see a change in inflection of the profile with high-Oersted field. This becomes more pronounced in 2(f), where the thickness is 100 μm. [The plot of surface angle with thickness in Fig. 3(b) is also similarly illustrative.] Also, going from panel 2(d) to 2(e)(e) to 2(f), the current density required to achieve comparable scissorlike deflection reduces to 1 order of magnitude—no longer 3 orders of magnitude, as in the thinner stripes. Thus, with sufficient thickness the character of the magnetization profile changes and Eq. (4b) no longer applies since it does not predict the described behavior.

Denoting the point of change in inflection as z_i, defined by $\ddot{\theta}(z_i)=0$—the point at which $\ddot{\theta}(z)$ changes sign—Eq. (3a), for the case $H_{\text{Zeeman}}=0$, implies $z_i=-cK \sin \theta_i/2\pi M_0 J$, where $\theta_i<0$ is the angle of magnetization at z_i. Thus, when it exists, which is always the case when $J>cK/\pi M_0 d$, the point of change in inflection z_i is contained within the interval $0<z_i<cK/2\pi M_0 J$. When a change in inflection arises it is because saturation within the Oersted field tends to be localized at the stripe surfaces, a consequence of the Oersted field linearly approaching zero toward the center of the stripe, in accordance with Eq. (1). Thus, with sufficient thickness, a transition arises within the angular profile of magnetization between a regime of surface character (dominated by current and exchange) and one of bulk character (dominated by anisotropy, exchange, and dipole-dipole interactions) partitioned by z_i. In the spin wave analyses section, we shall discuss the implications of this localization effect on spin waves of the scissor state.

To realize the scale of this effect, consider Fig. 2(e), where we have a stripe of thickness $d=10$ μm. For the curve labeled 5 corresponding to current density $J=1.67\times10^8$ A/m^2, we see that the crossover between surface and bulk character occurs at about $z_i=1.4$ μm (3.6 μm from the surface). From our analysis above, this is within the stated upper limit for z_i given by $cK/2\pi M_0 J=1.74$ μm. For a stripe of width 25 times greater than its thickness, we have a cross-sectional area of current given by 10×250 μm^2, so the current in this case is $I=(1.67\times10^8$ A/m$^2)\times(10$ μm$)\times(250$ μm$)=0.4$ A, a value not unrealizable in these thicker stripes.

In Figs. 3(c) and 4 we show how an external field H_{Zeeman} applied along the easy axis tends to counter the angular deflection induced by the Oersted field. In Fig. 3(b) the surface magnetization tends to align readily with the Oersted field as the stripe thickness increases. In Fig. 3(c) a small external magnetic field of $H_{\text{Zeeman}}=8.0$ A/m$=0.1$ Oe can rotate the surface magnetization back toward the easy axis by an angular degree or more. The effect of the Zeeman field is further illustrated in Fig. 4 for a stripe of thickness $d=1000$ Å. Here, we plot the angle of the surface magnetization as a function of H_{Zeeman}, up to very high fields along the direction of current, for several values of current density J. The figure shows the approach of the magnetization to saturation in the applied field. The curves are always asymptotic to the zero of angle, but it is clear that saturation becomes increasingly difficult as J is augmented. In the spin wave analyses section, we develop the theory of linearized spin waves of the nonuniform magnetic ground state described above, presenting calculations of spin-wave excitations in the presence of the transport current as a function of stripe thickness.

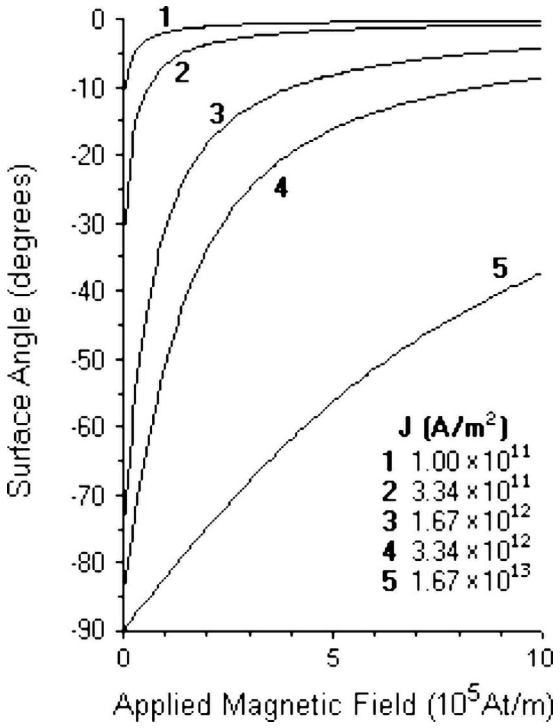

FIG. 4. Angle of deviation of magnetization from easy axis, at the top surface of a stripe of $d=1000$ Å in thickness, as a function of an external magnetic field H_{Zeeman} applied along this same axis. Curves are displayed for several values of current density J as indicated.

III. SPIN WAVE ANALYSES

A. Linearized spin-wave theory of the current-carrying ferromagnetic stripe

We present calculations of spin waves via the linearized Landau-Lifshitz equation of motion, wherein the time rate of change in local magnetization $\vec{M}(\vec{x},t)$ at a distance z from the center of the stripe is described by a precession of frequency Ω (with magnitude M_0 held fixed) about the ground-state orientation $\theta(z)$, as defined by Eq. (3). Specifically, the magnetization $\vec{M}(\vec{x},t)=M_0\hat{x}'(z)+\delta\vec{m}(\vec{x})\cdot\exp(-\Omega t)$ experiences a torque exerted by an effective magnetic field $\vec{H}_{\text{eff}}(\vec{x},t)=H_0(z)\hat{x}'(z)+\delta\vec{h}(\vec{x})\cdot\exp(-\Omega t)$, where

$$H_0(z)=-\frac{2A}{M_0}\dot{\theta}(z)^2+\frac{2K}{M_0}\cos^2\theta(z)+H_J(z)\sin\theta(z)+H_{\text{Zeeman}}\cos\theta(z) \tag{5}$$

is the magnitude of the ground-state effective field. Here, we have introduced a rotation by angle $\theta(z)$ about the z axis, one that transforms Cartesian coordinates of x and y at z into $x'(z)$ and $y'(z)$ such that we can define new unit vectors,

$$\hat{x}'(z)=\cos\theta(z)\hat{x}+\sin\theta(z)\hat{y},$$

$$\hat{y}'(z)=-\sin\theta(z)\hat{x}+\cos\theta(z)\hat{y}, \tag{6}$$

as in Fig. 1. Thus, the magnetic ground state at z is aligned with the $\hat{x}'(z)$ axis and the dynamical terms $\delta\vec{m}(\vec{x})$ and $\delta\vec{h}(\vec{x})$, taken to first order in the equation of motion, have components of relevance in the $\hat{y}'(z)$ and z directions. With the addition of a transformation to right and left circularly polarized components,

$$\delta m_{\pm}(\vec{x}) = \delta m_{y'}(\vec{x}) \pm i\,\delta m_{z}(\vec{x}), \quad \delta h_{\pm}(\vec{x}) = \delta h_{y'}(\vec{x}) \pm i\,\delta h_{z}(\vec{x}), \tag{7}$$

the equation of motion, with gyromagnetic ratio γ and Gilbert damping constant λ, can be expressed in two-component form as

$$\frac{1}{\gamma}\Omega\,\delta m_{\pm}(\vec{x}) = \mp\left[H_0(z) + i\frac{\lambda\Omega}{\gamma M_0}\right]\delta m_{\pm}(\vec{x}) \pm M_0\,\delta h_{\pm}(\vec{x}). \tag{8}$$

When the magnetization deviates from its ground-state orientation local magnetic-dipole moments within the volume of the stripe and at its surfaces generate an overall dipolar field $\delta\vec{h}^{(\mathrm{dip})}(\vec{x})$ whose time-dependent form is additive to the Oersted field of Eq. (1), such that the total demagnetizing field can be written as $\vec{H}(\vec{x},t)=H_J(z)\hat{y}+\delta\vec{h}^{(\mathrm{dip})}(\vec{x})\cdot\exp(-\Omega t)$. The field $\delta\vec{h}^{(\mathrm{dip})}(\vec{x})$ is derived in the Appendix. Hence, the components $\delta h_{\pm}(\vec{x})$ of the dynamical effective field, which express variations in exchange, anisotropy, and demagnetizing fields, can be written as

$$\delta h_{\pm}(\vec{x}) = \frac{2A}{M_0^2}\nabla^2\delta m_{\pm}(\vec{x}) + \frac{H_1(z)}{M_0}[\delta m_{+}(\vec{x}) + \delta m_{-}(\vec{x})] + \delta h_{\pm}^{(\mathrm{dip})}(\vec{x}), \tag{9}$$

where we have made the definition

$$H_1(z) = -\frac{A}{M_0}\dot{\theta}(z)^2 + \frac{K}{M_0}\sin^2\theta(z). \tag{10}$$

The term proportional to $H_1(z)$ in Eq. (9) arises in the presence of the transport current because the ground state, as we have shown in the magnetic ground state section, is nonuniformly distributed across the thickness of the stripe in the scissorlike arrangement defined by $\theta(z)$. Therefore, $H_1(z)$ vanishes only when $\theta(z)\equiv 0$, the uniform case.

Upon substitution of Eq. (9), Eq. (8) can be Fourier transformed with respect to the in-plane variables x and y, resulting in expressions in terms of continuous variables k_x and k_y, with $\vec{k}_{\|}=k_x\hat{x}+k_y\hat{y}$. In this way, within the interior of the stripe, we have

$$\frac{\Omega}{\gamma}\delta m_{\pm}(\vec{k}_{\|},z) = \mp\left[\frac{i\lambda\Omega}{\gamma M_0} + H_0(z) - H_1(z) + \frac{2A}{M_0}\left(k_{\|}^2 - \frac{\partial^2}{\partial z^2}\right)\right] \times \delta m_{\pm}(\vec{k}_{\|},z) \pm H_1(z)\,\delta m_{\mp}(\vec{k}_{\|},z) \pm M_0\,\delta h_{\pm}^{(\mathrm{dip})}(\vec{k}_{\|},z). \tag{11}$$

The Fourier coefficients $\delta h_{\pm}^{(\mathrm{dip})}(\vec{k}_{\|},z)$ of the dipolar field are derived in the Appendix and are given by Eq. (A5). The boundary conditions are those consistent with our model,[17] viz.,

$$\left.\frac{\partial}{\partial z}\delta m_{+}(\vec{k}_{\|},z)\right|_{z=\pm z_0} = 0, \qquad \left.\frac{\partial}{\partial z}\delta m_{-}(\vec{k}_{\|},z)\right|_{z=\pm z_0} = 0. \tag{12}$$

Equation (11), taken together with Eqs. (12) and (A5), expresses the eigenvalue problem of Ω and $\delta m_{\pm}(\vec{k}_{\|},z)$ in terms of two coupled integrodifferential equations of second order. We next discuss the solutions.

B. Calculations of spin waves in the presence of an applied current

We solved Eqs. (11) and (12) using a finite-difference method, wherein the dipolar integrals of Eq. (A5) can be approximated by Gauss-Legendre quadrature. Our technique is similar to that used in the numerical solution of homogenous Fredholm equations.[18] This numerical approach allows us to address the dipolar integrals on a grid of $n=1,2,\ldots,N$ points z_n that are nonuniformly distributed across the thickness of the stripe, in accordance with the quadrature algorithm. On this N-point mesh, the outermost $(n=1,N)$ circularly polarized components of dynamical magnetization satisfy the four boundary conditions of Eq. (12) while the remaining interior components form $2N-4$ homogeneous finite-difference equations. From the characteristic equation of these $2N-4$ degrees of freedom we can obtain spin waves of the rectangular geometry.

Specifically, the above finite-size mesh approximates the longest wavelengths of undulation of $\delta m_{\pm}(\vec{k}_{\|},z)$ across the thickness of the stripe. As a consequence, linear diagonalization on this N-point mesh of the $2N-4$ interior finite-difference equations captures the lowest-lying positive bulk spin-wave frequencies (and their highest-lying negative-value counterparts). As the density of the N-point mesh increases or equivalently as the dimension $2N-4$ of the corresponding dynamical matrix increases, accuracy of estimation of these lowest-lying modes improves, and diagonalization captures yet more higher-lying bulk spin-wave bands. In theory, as N approaches infinity, one attains a solution of the entire bulk spin-wave manifold, assuming a converging calculation of the dipolar integrals can be achieved. In practice, one establishes a value of N sufficiently large so as to accurately estimate the lowest-lying spin-wave bands of interest. Additional best practices, such as extrapolation from multiple mesh sizes, can be exploited to improve accuracy and quantify the error of estimate.

For each $\vec{k}_{\|}$ of interest we estimated bulk spin-wave solutions $\Omega^{(s)}(\vec{k}_{\|})$ and $\delta m_{\pm}^{(s)}(\vec{k}_{\|},n)$, where $s=\pm 1,\pm 2,\ldots,\pm(N-2)$, by solving the linear eigenvalue problem[19] on the N-point mesh, with mesh points chosen via Gauss-Legendre quadrature. The results reported here are for the model parameters used in our earlier ground-state calculations, appropriate for Permalloy. In addition, we set the Gilbert damping constant λ to zero to simplify our presentation. We estimated bulk spin-wave modes using mesh sizes of 32, 64, and 128. The 32-point mesh resulted in errors of about 1% or less while the 64-point mesh usually gave errors of about one-tenth of 1%. The greatest errors incurred were typically for

large current densities and high-lying bands at short wavelengths, and these were sufficiently addressed by the 64-point mesh, although in a few instances, as noted below, we required the 128-point mesh.

Before we present calculations of spin waves in the presence of an applied current, we consider the spin-wave dispersion of the uniformly magnetized stripe with $H_{\text{Zeeman}}=0$. This serves to illustrate the effectiveness of our numerical technique as well as provide a brief review of the spin-wave theory of the zero-current limit. Appropriate for thin stripes, a long-wavelength approximation of the dispersion of the lowest-lying spin-wave band[20] is

$$\frac{1}{\gamma}\Omega^{(1)}(\vec{k}_{\|}) \cong \sqrt{\left(H_0 + 2\pi M_0 \frac{k_y^2}{k_{\|}} d + \frac{2A}{M_0} k_{\|}^2\right)\left(H_0 + 4\pi M_0 - 2\pi M_0 k_{\|} d + \frac{2A}{M_0} k_{\|}^2\right)}, \tag{13}$$

where by H_0 we mean Eq. (5) with $\theta(z)\equiv 0$, i.e., $H_0 = 2K/M_0$. In Fig. 5(a) we used our numerical approach (a mesh of size 32) to plot the lowest-lying bulk spin-wave band of a stripe of thickness $d=1000$ Å, showing the dispersion along the positive x direction. Equation (13) is superimposed (labeled as curve "A") to illustrate the agreement between our numerical approach and this long-wavelength approximation. In Fig. 5(b), using the same numerical parameters, we plot the dispersion along the y direction for the four lowest-lying bulk spin-wave bands. Again, Eq. (13) is superimposed as curve A for comparison. Figure 5(b) also shows hybridization between spin-wave states of adjacent bands—points at which there is mixing between degenerate states. These points of hybridization are indicative of the evolution of the Damon-Eshbach surface mode[14] into the bulk spin-wave manifold and, thus, demonstrate that the surface mode can be inferred from knowledge of bulk modes. Figure 5(c) shows this hybridization at higher resolution among the three lowest bands.

To illustrate this, consider the frequency of the Damon-Eshbach mode[14] as it propagates along the y direction; in our model this well-known result[14] can be written as

$$\frac{1}{\gamma}\Omega^{(\text{surf})}(0,k_y) = \sqrt{(H_0 + 2\pi M_0)^2 - 4\pi^2 M_0^2 \exp(-2|k_y|d)}. \tag{14}$$

Thus, in Fig. 5(b) we also superimpose a plot of Eq. (14), labeled as curve "B," which is bounded below by $\sqrt{H_0(H_0+4\pi M_0)} \cong 1.91\times 10^{-2}$ T=191 G and above by $H_0 + 2\pi M_0 \cong 5.01\times 10^{-1}$ T=5010 G. Note how the plot of Eq. (14) matches the points of hybridization between the various low-lying bulk spin-wave bands as it asymptotically settles into a position between the second and third bands. Again, the numerical calculation is performed on a single mesh of size $N=32$. The accuracy of our results is a testament to Gauss-Legendre quadrature, which efficiently accounts for the contributions of the integrals of the dipolar-field components of Eq. (A5).

We now turn to a discussion of spin waves in the presence of the transport current. Figure 6 depicts the dispersion of the lowest-lying spin-wave band of a relatively thin stripe of thickness $d=100$ Å, as a function of applied current, with $H_{\text{Zeeman}}=0$. [The corresponding magnetic ground-state configurations are illustrated in Fig. 2(b).] Figure 6(a) shows the dispersion along the easy axis; Fig. 6(b) shows this dispersion with $k_y=2.0\times 10^7$ m^{-1}; and Fig. 6(c) shows the dispersion along the y axis, perpendicular to the easy direction. Generally speaking, the application of current raises the frequencies of states, stiffening the spin-wave response of the thin stripe. As the current density is increased to $J=1.0\times 10^{14}$ A/m^2 a noticeable asymmetry emerges with respect to the easy axis, as seen in Fig. 6(a)—the dispersion curve is lowered in the direction of applied current and raised opposite the direction of applied current. In our concluding remarks we discuss the nature of this asymmetry further.

However, the stiffening effect shown in Fig. 6 does not hold for thicker stripes. In Fig. 7(a) we plot the lowest-lying standing-wave resonance frequency as a function of current density J for a range of stripe thicknesses d. Consistent with Fig. 6, this resonance frequency increases monotonically with increasing J as long as the stripe thickness is much less than a critical value of $d_c=1.55$ μm. Note that for $d=1$ μm the curve of "4" has a minimum due to its proximity to the thickness of criticality. However, when the stripe thickness exceeds the critical value, the lowest-lying resonance frequency always goes soft. In Fig. 7(a), curves 5 and 6 go to zero at critical current densities $J=4.65\times 10^7$ A/m^2 and $J=4.16\times 10^6$ A/m^2, respectively, and these frequencies remain at zero as J continues further, until eventually we see once again a stiffening of the resonance frequency—curves 5 and 6 again emerge to positive values. In other words, when stripe thickness exceeds d_c the instability is manifested as a gap in current density, which is more fully displayed in Fig. 7(b). Thus, in low-Oersted fields the quasiferromagnetic scissor state is stable, followed by a range of current densities in which this state becomes unstable, followed by a region of very high-Oersted fields within which stability is restored. Note still further that even the high-Oersted field state becomes unstable as J increase without bound, characterized by a discontinuous drop to zero. This occurs at the limit of the reliability of our numerical calculations.

Before we turn to an explanation of this behavior, in Fig. 8 we explore further the manner in which low-lying spin-wave frequency softens for these two particular stripe thicknesses. In both cases of stripe thickness ($d=10$ μm and d

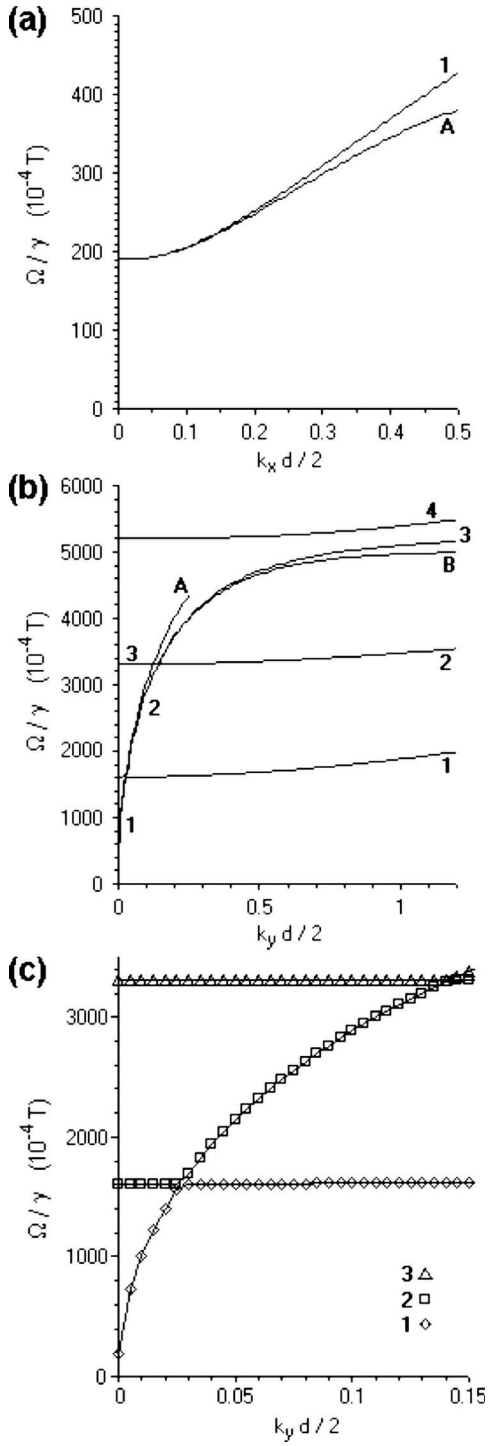

FIG. 5. Numerical calculation of dispersion in the positive x and y directions for a uniformly magnetized stripe of $d=1000$ Å thickness. In (a) the long-wavelength approximation of Eq. (13) is superimposed as a curve labeled A on the lowest-lying spin-wave band labeled "1." In (b) Eq. (13) is again superimposed as the curve labeled A but also shown is hybridization among the four lowest-lying spin-wave bands labeled 1–4, which is indicative of formation of the Damon-Eshbach surface mode (Ref. 14), whose frequency is superimposed via Eq. (14) as the curve labeled B. In (c) the scale is made smaller and shows points of calculation of the three lowest bands, illustrating the fineness of calculation. All plots were determined from a single 32-point mesh.

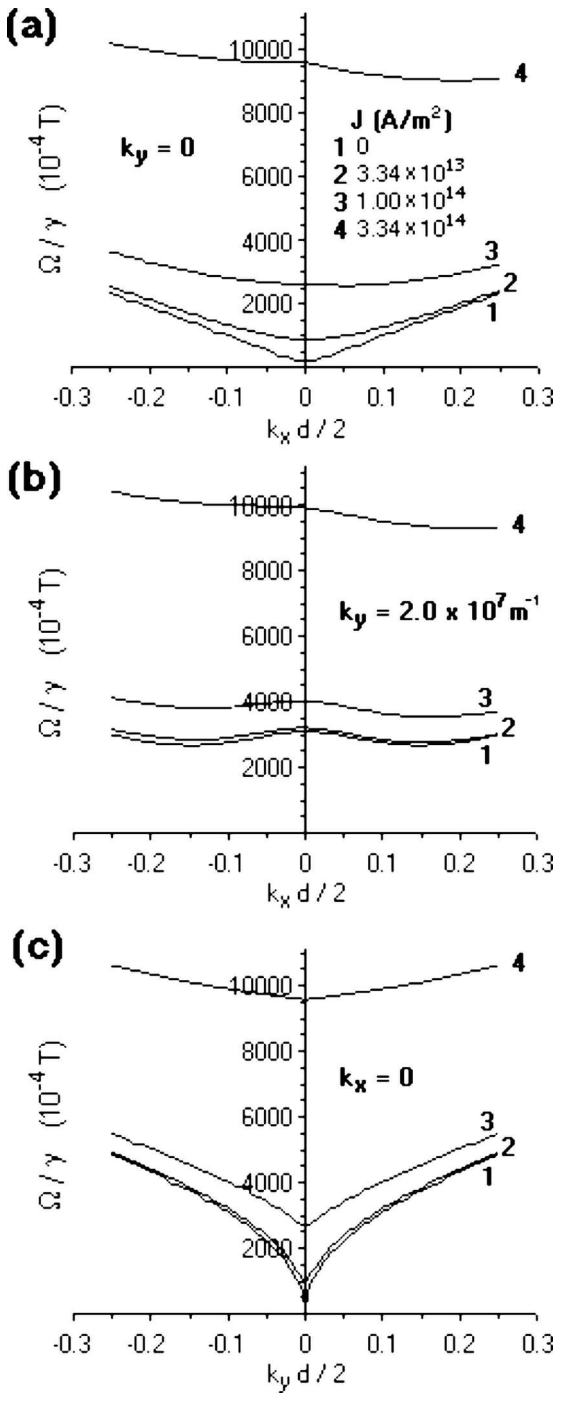

FIG. 6. Spin-wave dispersion of the lowest-lying band (thickness $d=100$ Å) for values of applied current density J as indicated. Panels show cross sections of (a) $k_y=0$, (b) $k_y=2.0\times10^7$ m^{-1}, and (c) $k_x=0$. As current increases, stiffening of spin-wave response is evident, as is asymmetry along the easy x axis. Calculations were performed on a 64-point mesh.

$=100$ μm) we see that as the current density increases toward criticality it is the resonance frequency, at $\vec{k}_\parallel=0$, that initially goes to zero. Beyond this current density, the resonance frequency remains fixed at zero and a k-space gap, i.e., $\Omega^{(1)}(\vec{k}_\parallel)<0$ [not to be confused with the current-density gap of Fig. 7(b)], opens up in the spin-wave spectrum, initially

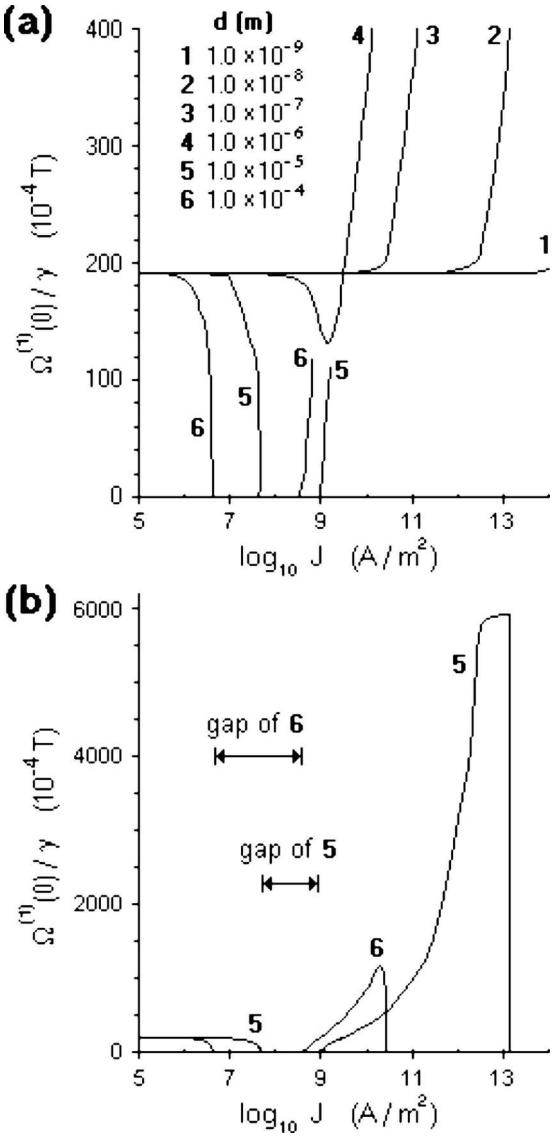

FIG. 7. Lowest-lying standing-wave resonance frequency, i.e., $\vec{k}_{\parallel}=0$, as a function of current density J, plotted on a base-ten logarithmic scale, for a range of thicknesses d. In (a), for thin stripes the frequency stiffens with applied current, monotonically increasing from a value of $\Omega^{(1)}(0)/\gamma=1.91\times10^{-2}$ T=191 G, corresponding to the uniformly magnetized stripe. For thicker stripes, beginning at $d_c=1.55$ μm, the frequency softens to zero, indicative of an unstable scissorlike ground state. The zero frequencies shown in (a) correspond to $J=4.65\times10^7$ A/m^2 (for $d=10$ μm) and $J=4.16\times10^6$ A/m^2 (for $d=100$ μm). As J is increased further, as seen more fully in (b), the frequency in each case once again stiffens. Calculations were performed on a 64-point mesh, except near the instability, where a 128-point mesh was required.

along the direction of current, over an interval $0<k_x<k_x^{(c)}$, with width $k_x^{(c)}$ that increases with increasing J. This is illustrated in Fig. 9(a) for the $d=10$ μm stripe, where $J=4.67\times10^7$ A/m^2 and initially $k_x^{(c)}=4.04\times10^4$ m^{-1}. Figure 9(a) depicts the spin-wave k-space gap and how this gap is made to diminish with increasing Zeeman field H_{Zeeman} applied along the direction of current. Figure 9(b) shows the corresponding scissor-state configurations for each value of

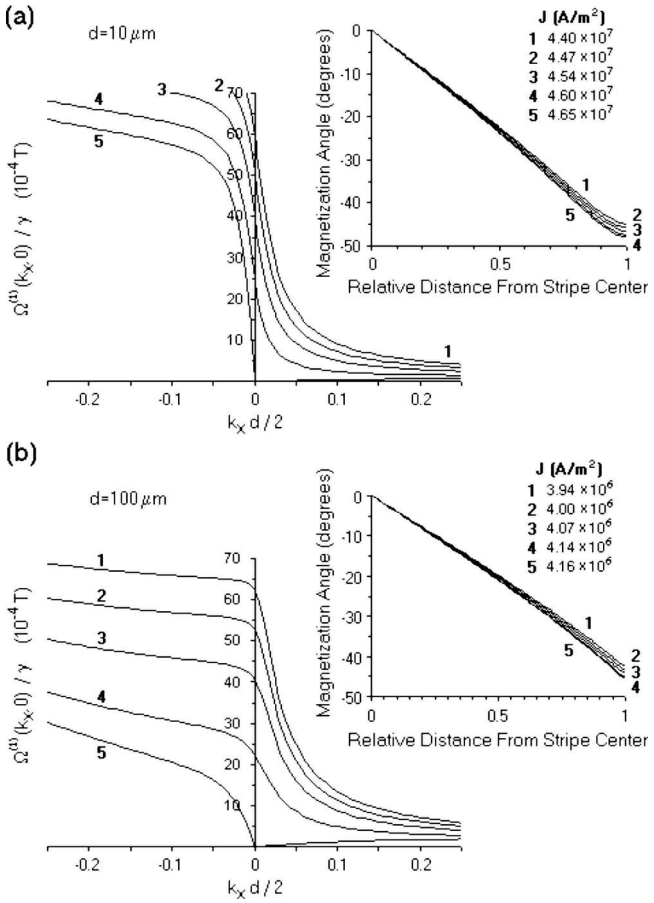

FIG. 8. Dispersion of lowest-lying spin-wave band for several values of current density J, as indicated, along the easy direction. Inset shows corresponding magnetic ground states. Results are for thicknesses (a) $d=10$ μm and (b) $d=100$ μm. In either case, the dispersion first goes to zero at $\vec{k}_{\parallel}=0$, where $J=4.65\times10^7$ A/m^2 (for $d=10$ μm) and $J=4.16\times10^6$ A/m^2 (for $d=100$ μm), as in Fig. 7. Calculations were performed on a 128-point mesh.

H_{Zeeman} considered. Thus, Fig. 9 illustrates that the scissorlike magnetic ground state becomes unstable, and it shows how an external field applied along the direction of current can stabilize it.

To understand the cause of the magnetic instability we note that above the critical stripe thickness d_c the Oersted field has two distinctly different influences on magnetic order, attributable to its tendency to pin the magnetization at either surface into orientations antiparallel and perpendicular to the easy axis, which give rise to the current-density gap seen in Fig. 7(b). As current is increased from zero, the pinning effect of the Oersted field at first is localized to the stripe surfaces since it vanishes at the center of the stripe. Nevertheless, the low-Oersted field exerts an influence over the interior of the stripe by distorting the ferromagnetic state into a scissor configuration, as we saw in our earlier ground-state analysis, which weakens the restoring effect of exchange under excitations of the ground state. Thus, as current increases, excitations of the ground state, strongly dipole-dipole in nature via Eq. (A5), eventually become unstable and persist over a range of current densities. However, as the current continues to increase, the strength of the Oersted field

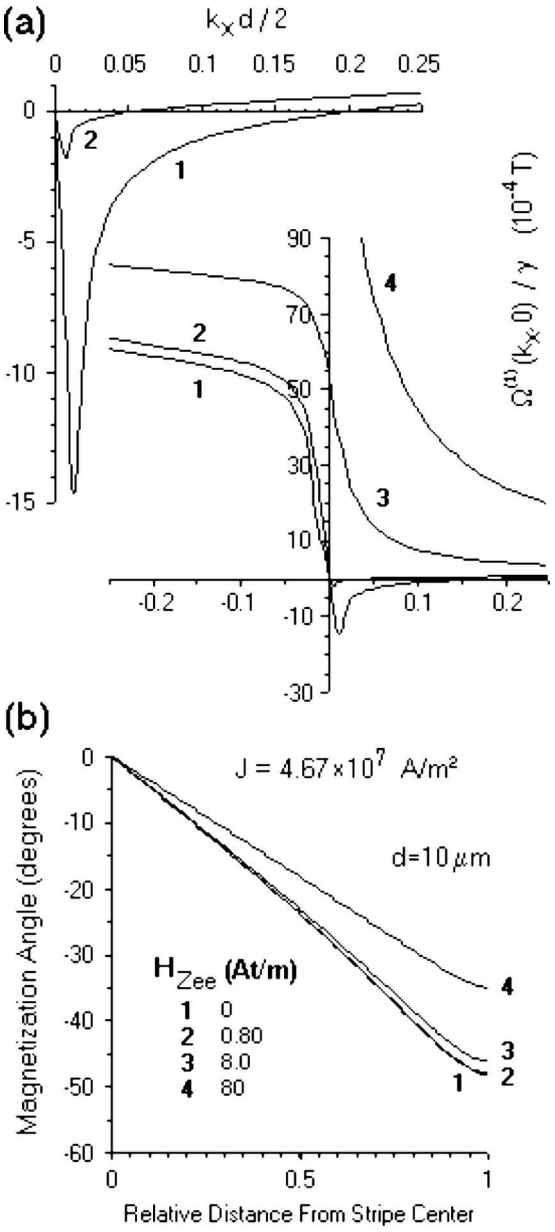

FIG. 9. In (a) the instability of the scissorlike magnetic ground state is shown as a gap in the long-wavelength spectrum of the lowest-lying spin-wave band, along the easy axis, in the direction of applied current. The current density is $J=4.67\times10^7$ A/m^2, the stripe thickness is $d=10$ μm, and the gap extends over the interval $0<k_x<4.04\times10^4$ m^{-1}. Plotted is the spin-wave dispersion for several values of increasing external field H_{Zeeman}, applied along the direction of current, illustrating the stabilizing affect of this field. The inset depicts the behavior at larger scale. In (b) the angle of magnetization of the scissor state is shown across the thickness of the stripe for the values of applied field considered in (a). Calculations were performed on a 128-point mesh.

grows proportionally and begins to exert a stronger influence within the center of the stripe, with respect to the dynamical dipole fields that can exist there. Thus, in very high-Oersted fields, we see the restoration of long-range order, driven by the Oersted field itself, which has encroached upon the interior of the stripe. In this regime, magnetization is pinned perpendicular to the easy axis, to great depth within the stripe, such that the scissor ground state may be viewed as two antiparallel domains separated by a Néel wall. Finally, as the applied current increases without bound the Néel domain wall becomes exceedingly thin, and the domain structure becomes once again unstable.

It is of interest to examine the spin-wave eigenvectors $\delta m_{\pm}(\vec{k}_{\parallel},z)$ as the current density is increased from zero and through the region of instability of the magnetic ground state, as this sometimes provides inference about the form taken by the new long-range order within the region of instability. With $H_{\text{Zeeman}}=0$, these eigenvectors are illustrated in Fig. 10 for the stripe of thickness $d=10$ μm. Figures 10(a)–10(c)are representative of the low-Oersted-field scissor state, Fig. 10(d) depicts eigenvectors corresponding to Fig. 9, panels 9(e) and 9(f) are representative of the current-density gap of Fig. 7(b), and panels 7(g) and 7(h) are associated with the stable state of the high-Oersted-field limit. In Fig. 10(a), corresponding to zero applied current, the right and left circularly polarized components have amplitudes that are uniform across the thickness of the stripe. The amplitudes are nearly identical because the anisotropy field $H_0=2K/M_0(3.6$ G) is so much smaller than the demagnetizing field $4\pi M_0$ (10 020 G). Thus, precessional motion is nearly restricted to a plane parallel to the stripe surfaces. As the current density is increased this motion becomes localized to the center of the stripe, the result of pinning by the Oersted field, concentrated at the surfaces. By panel 10(d), at a current density beyond the first point of instability, the amplitudes of the eigenvectors become numerically indistinguishable, indicative of a purely in-plane precessional motion. This is seen also within the current-density gap, as illustrated in Fig. 10(f). Purely out-of-plane precessional motion is also exhibited within the gap, as depicted in Fig. 10(e), toward the low end, but not continuously with increasing J. However, as the current density is increased beyond the gap, we again find eigenvectors in panels 10(g) and 10(h) like those of panels10(c) and 10(d), albeit increasingly isolated to the center of the stripe, due to the overwhelming Oersted pinning field. Recalling the onset of instability at $\vec{k}_{\parallel}=0$, in Fig. 8, there is no immediately recognizable length scale associated with new long-range order. We note, however, that Bergmann *et al.*[21] recently proposed a model of long-range order to address frustrated magnetization in Co nanowires that arises from competing interactions not unlike those described here. While inferences drawn from this earlier work are limited, particularly given the differences in geometry, we nevertheless find the magnetic instability of the present case to be an interesting topic worthy of future study.

As a last topic we investigate the influence of the transport current on the Damon-Eshbach surface mode[14] of a stripe of thickness $d=1000$ Å. Recall from Fig. 5 the form of this mode when the stripe is uniformly magnetized. Now consider how this mode is modified when a dc electric current is applied along the easy axis. In Fig. 11 we show the first few low-lying bands of the bulk spin-wave manifold as a function of increasing current density. In Fig. 11(a), as current is increased to $J=1.00\times10^{11}$ A/m^2, the frequency of propagation of the surface mode along the y direction

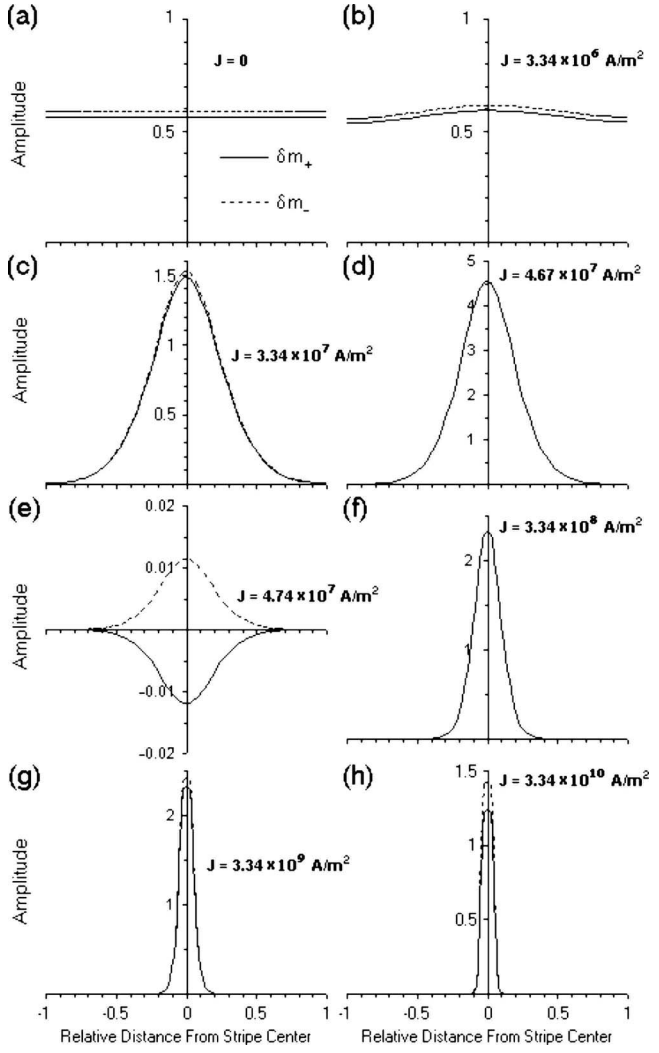

FIG. 10. Plot of right and left circularly polarized eigenvectors $\delta m_{\pm}^{(s)}(\vec{k}_{\parallel},z)$, with $H_{\text{Zeeman}}=0$, corresponding to the lowest-lying ferromagnetic resonance of the stripe of thickness $d=10$ μm, for several values of increasing current density J, as indicated. As current density increased from zero precessional motion becomes confined to the center of the stripe, a result of increased pinning by the Oersted field at the surfaces. By panel (d), corresponding to the current density of the instability described in Fig. 9, the right and left components of circular polarization become numerically indistinguishable. Panels (e) and (f) depict eigenvectors within the instability gap of Fig. 7(b). Panels (g) and (h) correspond to the high-Oersted-field limit. The calculations were performed on a 64-point mesh.

diminishes only very slightly, but along the $+x$ direction there is increased hybridization of bulk states, indicating that the surface mode has assumed a direction of propagation in this orientation. In Fig. 11(b), as current is increased further to $J=3.34\times10^{11}$ A/m^2, hybridization of bulk states, corresponding to propagation in the $-x$ direction, is seen also—hybridization of states along the x direction is therefore markedly asymmetric. When the current density reaches $J=1.67\times10^{12}$ A/m^2, in Fig. 11(c), propagation along the y direction is seen to diminish significantly.

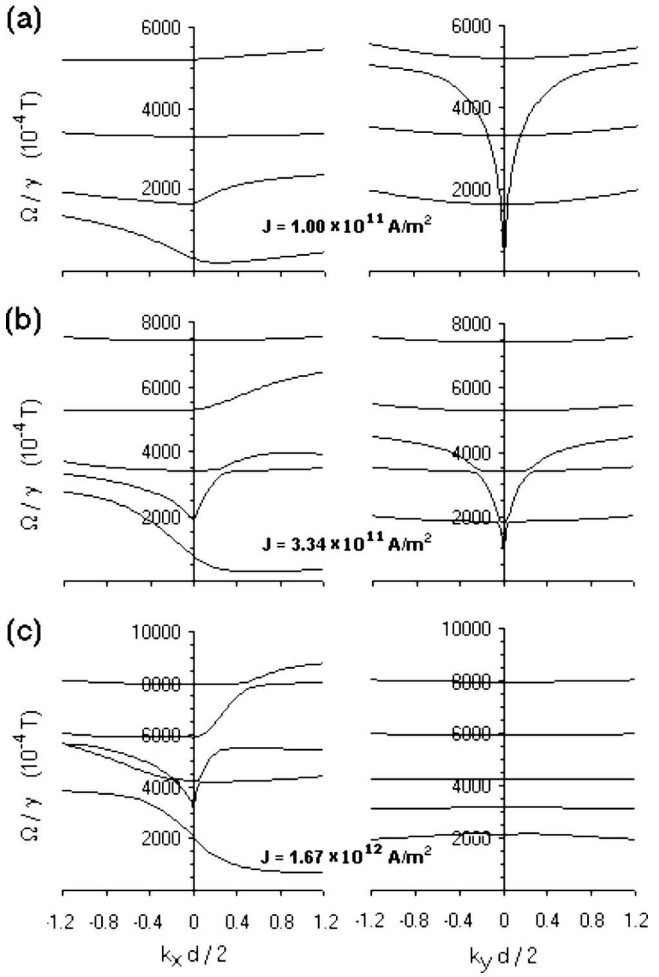

FIG. 11. Evolution of the Damon-Eshbach surface mode (Ref. 14) with increasing current density J. Displayed is the spin-wave dispersion of bulk modes along the x and y directions. In (a) $J=1.00\times10^{11}$ A/m^2, in (b) $J=3.34\times10^{11}$ A/m^2, and in (c) $J=1.67\times10^{12}$ A/m^2. Calculations were performed on a 32-point mesh.

A qualitative explanation of the above behavior follows by noting that Eq. (A5) depends on a rotated wave vector. As current is increased, the direction of propagation of the Damon-Eshbach surface mode[14] is rotated toward the easy axis, as illustrated in Fig. 12. Panel (a) of this figure illustrates the case of the surface mode localized to the top surface, which tends to propagate in the $+y$ direction. Panel (b) illustrates the surface mode localized to the bottom surface, which tends to propagate in the $-y$ direction. In our simplified picture we treat the scissor ground state as a hard magnetization in each half of the stripe. Thus, there is a rotation of one sense in one half of the stripe and a rotation in the opposite sense in the other half of the stripe, corresponding to a hard scissorlike configuration. Since the surface mode tends to propagate perpendicular to the magnetization, the direction of propagation is rotated in one sense in one half of the stripe and rotated in the opposite sense in the other half of the stripe, as illustrated in each of the two panels.

For example, with regard to Fig. 12(a), in the top half of the stripe the surface mode tends to form a component of

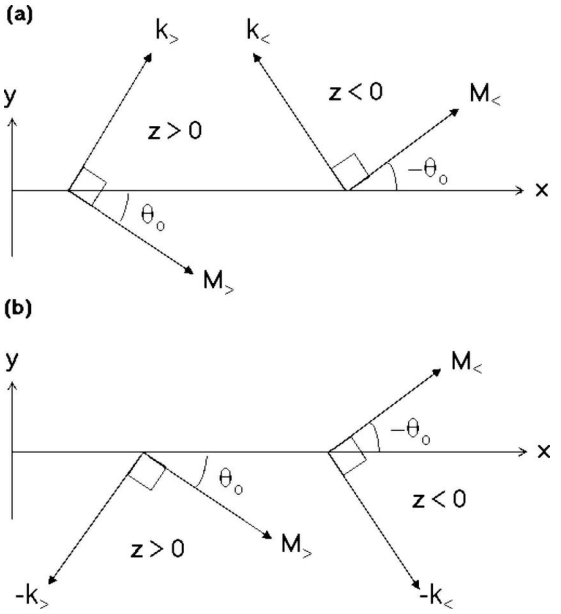

FIG. 12. Sketch of the current-induced rotation of the direction of propagation of the Damon-Eshbach surface mode (Ref. 14) within each half of the stripe. Each half of the stripe is approximated by a hard magnetization of angle $\pm\theta_0$ with respect to the easy (x) axis. Panel (a) refers to the Damon-Eshbach surface mode (Ref. 14) propagating in the $+y$ direction, along the top, i.e., $z>0$, surface. Panel (b) refers to the Damon-Eshbach mode (Ref. 14) propagating in the $-y$ direction, along the bottom, i.e., $z<0$, surface. In each panel, propagation along the easy axis tends to favor the direction of applied current, i.e., the $+x$ direction, because of the surface to which the mode is localized in each case.

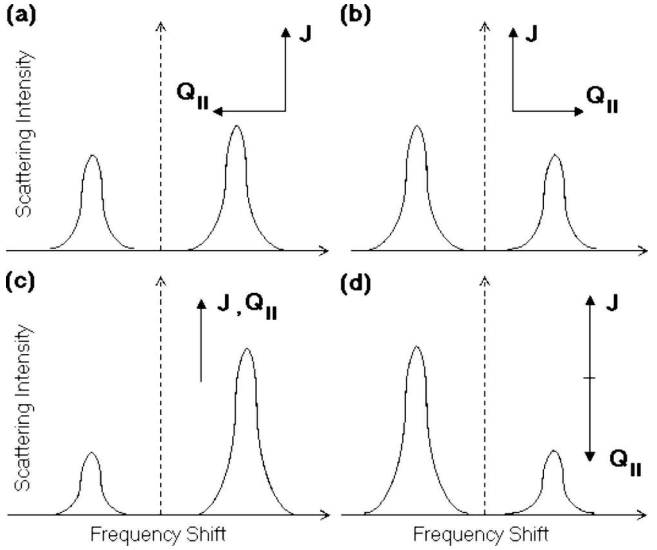

FIG. 13. In idealized sketch of the BLS intensity of the surface excitation one would expect to observe in the presence of a current density J applied along the $+x$ easy direction. Here, $\vec{Q}_{\parallel}$ is the transfer wave vector denoting the direction of incident light relative to the direction of J. Backscattering is in the $-\vec{Q}_{\parallel}$ sense. Panels (a) and (b) depict the typical Stokes and anti-Stokes features of the stripe geometry whereas panels (c) and (d) correspond to intensity features specific to the current-injected ferromagnetic stripe. These later features result from the rotation of the direction of propagation of the Damon-Eshbach surface mode (Ref. 14) into the easy axis; the larger (smaller) peak is associated with rotation into (away from) the applied current. The intensities of the peaks of panels (a) and (b) decrease with increasing applied current whereas those of panels (c) and (d) increase with increasing applied current.

wave vector projected into the $+x$ direction, in addition to the $+y$ component, whereas in the bottom half of the stripe the tendency is to form a component in the $-x$ direction, in addition to the $+y$ component. Because the mode is localized to the top half of the stripe, there is a stronger sense of propagation in the $+x$ direction—the direction of applied current—than in the $-x$ direction. Similarly, in Fig. 12(b), the tendency in the top (bottom) half of the stripe is to form a projection of wave vector in the $-x(+x)$ direction, in addition to the $-y$ component. Since the surface mode of Fig. 12(b) is localized to the bottom surface, the surface mode, again, tends to have a stronger component of propagation in the direction of applied current.

Thus, the net result of the applied current, consistent with 180° rotational symmetry about the easy axis, is the appearance of a spin-wave excitation that is localized to *both* surfaces of the stripe and that propagates most strongly along the direction of current, at the expense of propagating in the y direction, akin to a rotation of the direction of propagation of the Damon-Eshbach surface mode[14] into the x axis. The overall behavior is manifested in Fig. 11 as the appearance of asymmetrical hybridization along the x axis with increasing applied current, with diminished hybridization seen along the y direction. Thus, the sense of direction of propagation of the surface excitation shifts from the y axis to the x axis, with the caveat that it is no longer bound to a single surface because the new state is a rotated mix of the zero-current surface solution and its counterpart under time reversal.

In Fig. 13 we sketch the scattering intensity attributable to the surface excitation that one should observe in a BLS experiment. Figures 13(a) and 13(b) are the usual Stokes and anti-Stokes features observed via backscattering, along the direction perpendicular to the applied current, where the lesser feature corresponds to exciting the mode localized at the far surface, assuming a stripe sufficiently thin that the back-surface signal is detectable. With increasing current, both of these features will diminish, in accordance with the results of Fig. 11. On the other hand, panels 13(c) and 13(d) represent asymmetric features specific to the current-injected ferromagnetic stripe, as sketched in Fig. 12. The larger peak corresponds to excitation of the surface mode along the direction of current, originating from the near surface; the smaller peak is associated with propagation opposite the current, originating from the far surface, again assuming a stripe sufficiently thin. The intensity of these peaks increases with increasing applied current.

IV. CONCLUDING REMARKS

We have presented a theory of spin waves of a current-injected rectangular ferromagnetic stripe treated as a slab of infinite extent. In our analyses we employed an exact nu-

merical treatment of the dipolar field of the film geometry, which allowed us to calculate spin-wave excitations for a large range of stripe thicknesses and highly nonuniform ground-state configurations, in the presence of a transport current. Our numerical approach has application to micromagnetic calculations associated with other geometries under similar circumstances of applied current.

Among our results, we found that a dc electric current of sufficient strength applied along the easy axis can generate an asymmetry in the spin-wave dispersion, particularly along this same easy direction, characterized by a decreasing (increasing) slope with (against) the direction of applied current. This is similar in character to the spin-wave dispersion asymmetry associated with the Doppler shift of d electrons in itinerant ferromagnets;[22] however, it is an entirely different mechanism arising from the interaction of the magnetization with an Oersted field. Specifically, dynamical dipole-dipole interactions, embodied by Eq. (A5), give rise to our asymmetry, as a consequence of the scissoring of ground-state magnetization and subsequent formation of a Néel wall within the center of the stripe.

Another mechanism of spin-wave-dispersion asymmetry recently proposed by Mills and Dzyaloshinskii[23] has its origin in the flexoelectric interaction,[24] which involves the interaction of an electric field (due to electric polarization within a Néel wall) with the spatial gradients of nonuniform magnetization. In their study, Mills and Dzyaloshinskii discussed a spin-wave-dispersion asymmetry that is strongest perpendicular to both the electric field and easy axis, unlike the character of our asymmetry. They also show that the flexoelectric interaction gives rise to an instability, from which a new cycloidal magnetic state forms, which has some analogy to the instability we have described here.

Thus, in particular, we described an instability that arises in the magnetic scissor state with applied current and sufficient stripe thickness. For Permalloy stripes the critical thickness is equal to approximately 1 μm. In addition, we showed how, in thinner stripes, evolution of the Damon-Eshbach[14] is modified by the presence of the transport current, giving rise to surface-mode propagation along the direction of the applied current. We hope our approach and findings will stimulate further studies in this area.

ACKNOWLEDGMENTS

We would like to thank D. L. Mills and I. N. Krivorotov for helpful comments and suggestions. This research was supported by the National Institute of Standards and Technology through Purchase Order No. RA1341-08-SE-3214.

APPENDIX

The dipolar field that arises within our infinitely extended slab is the result of the excitation of local magnetic-dipole moments, both within the volume V of the stripe and at each of its two surfaces S. Respectively, the field contributions are

$$\delta\vec{h}_V^{(\mathrm{dip})}(\vec{x}) = \nabla \int_V \frac{\nabla' \cdot \delta\vec{m}(\vec{x}')}{|\vec{x}-\vec{x}'|} d^3x',$$

$$\delta\vec{h}_S^{(\mathrm{dip})}(\vec{x}) = -\nabla \oint_S \frac{\hat{n}' \cdot \delta\vec{m}(\vec{x}')}{|\vec{x}-\vec{x}'|} d^2x'_{\parallel}, \tag{A1}$$

where $\delta\vec{m}(\vec{x})$ is the dynamical part of the magnetization, $\hat{n}'$ is the outward unit normal to each surface S, $d^2x'_{\parallel}$ is an infinitesimal area of S, and $d^3x' = d^2x'_{\parallel}dz'$.

The Fourier coefficients of the above, the result of transformations with respect to the in-plane spatial coordinates, can be written as

$$\delta\vec{h}_V^{(\mathrm{dip})}(\vec{k}_{\parallel},z) = -\int_V \frac{\vec{x}'_{\parallel}+(z-z')\hat{z}}{|\vec{x}'_{\parallel}+(z-z')\hat{z}|^3}\left[ik_{y'}(z')\cdot\delta m_{y'}(\vec{k}_{\parallel},z') + \frac{\partial}{\partial z'}\delta m_z(\vec{k}_{\parallel},z')\right]\exp(-i\vec{k}_{\parallel}\cdot\vec{x}'_{\parallel})d^3x', \tag{A2a}$$

$$\delta\vec{h}_S^{(\mathrm{dip})}(\vec{k}_{\parallel},z) = \int_S \left[\frac{\vec{x}'_{\parallel}+(z-z_0)\hat{z}}{|\vec{x}'_{\parallel}+(z-z_0)\hat{z}|^3}\delta m_z(\vec{k}_{\parallel},z_0) - \frac{\vec{x}'_{\parallel}+(z+z_0)\hat{z}}{|\vec{x}'_{\parallel}+(z+z_0)\hat{z}|^3}\delta m_z(\vec{k}_{\parallel},-z_0)\right] \times\exp(-i\vec{k}_{\parallel}\cdot\vec{x}'_{\parallel})d^2\vec{x}'_{\parallel}, \tag{A2b}$$

where we define $k_{y'}(z) \equiv -k_x \sin\theta(z) + k_y \cos\theta(z)$. The integrals over in-plane coordinates can be evaluated in closed form, with the result

$$\delta\vec{h}_V^{(\mathrm{dip})}(\vec{k}_{\parallel},z) = 2\pi\int_{-z_0}^{z_0}\left[\frac{i\vec{k}_{\parallel}}{k_{\parallel}} - \mathrm{sgn}(z-z')\hat{z}\right] \times\left[ik_{y'}(z')\cdot\delta m_{y'}(\vec{k}_{\parallel},z') + \frac{\partial}{\partial z'}\delta m_z(\vec{k}_{\parallel},z')\right] \times\exp(-k_{\parallel}|z-z'|)dz', \tag{A3a}$$

$$\delta\vec{h}_S^{(\mathrm{dip})}(\vec{k}_{\parallel},z) = -2\pi\left[\frac{i\vec{k}_{\parallel}}{k_{\parallel}}+\hat{z}\right]\delta m_z(\vec{k}_{\parallel},z_0)\exp[k_{\parallel}(z-z_0)] + 2\pi\left[\frac{i\vec{k}_{\parallel}}{k_{\parallel}}-\hat{z}\right]\delta m_z(\vec{k}_{\parallel},-z_0)\exp[-k_{\parallel}(z+z_0)]. \tag{A3b}$$

Adding Eq. (A3) together and making use of Eq. (7), the components of circular polarization are

$$\delta h_{\pm}^{(\mathrm{dip})}(\vec{k}_{\parallel},z) = \pi\int_{-z_0}^{z_0}\left[\frac{-k_{y'}(z)}{k_{\parallel}} \pm \mathrm{sgn}(z-z')\right] \times\left\{k_{y'}(z')\cdot[\delta m_+(\vec{k}_{\parallel},z') + \delta m_-(\vec{k}_{\parallel},z')] - \frac{\partial}{\partial z'}[\delta m_+(\vec{k}_{\parallel},z') - \delta m_-(\vec{k}_{\parallel},z')]\right\} \times\exp(-k_{\parallel}|z-z'|)\cdot dz' - \pi\left[\frac{-k_{y'}(z)}{k_{\parallel}} \pm 1\right] \times[\delta m_+(\vec{k}_{\parallel},-z_0) - \delta m_-(\vec{k}_{\parallel},-z_0)]$$

$$\times \exp[-k_{\|}(z_0+z)] - \pi\left[\frac{k_{y'}(z)}{k_{\|}} \pm 1\right]$$
$$\times [\delta m_+(\vec{k}_{\|},z_0) - \delta m_-(\vec{k}_{\|},z_0)]$$
$$\times \exp[-k_{\|}(z_0-z)]. \quad \text{(A4)}$$

In Eq. (A4), the terms involving derivatives of the magnetization components can be eliminated via integration by parts. In this way, Eq. (A4) can be written as

$$\delta h_{\pm}^{(\mathrm{dip})}(\vec{k}_{\|},z) = \mp 2\pi[\delta m_+(\vec{k}_{\|},z) - \delta m_-(\vec{k}_{\|},z)]$$
$$+ \pi\int_{-z_0}^{z_0}\left[\frac{-k_{y'}(z)}{k_{\|}} \pm \mathrm{sgn}(z-z')\right]$$
$$\times [k_{y'}(z') + k_{\|}\,\mathrm{sgn}(z-z')]$$
$$\times \exp(-k_{\|}|z-z'|)\,\delta m_+(\vec{k}_{\|},z')\cdot dz'$$
$$+ \pi\int_{-z_0}^{z_0}\left[\frac{-k_{y'}(z)}{k_{\|}} \pm \mathrm{sgn}(z-z')\right]$$
$$\times [k_{y'}(z') - k_{\|}\,\mathrm{sgn}(z-z')]$$
$$\times \exp(-k_{\|}|z-z'|)\cdot \delta m_-(\vec{k}_{\|},z')\cdot dz', \quad \text{(A5)}$$

where we note cancellation of the surface terms. The leading terms of Eq. (A5) are those that contribute to ferromagnetic resonance (when one sets $\vec{k}_{\|}=0$), whereas the integrals strictly capture contributions associated with spin-wave dispersion.

*Correspondence: P.O. Box 14762, Scottsdale, Arizona 85267, USA.

[1] For early examples, see M. Johnson and R. H. Silsbee, Phys. Rev. B **37**, 5312 (1988); G. Prinz and K. Hathaway, Phys. Today **48**(4), 24 (1995); G. A. Prinz, Science **282**, 1660 (1998).

[2] M. N. Baibich, J. M. Broto, A. Fert, F. Nguyen Van Dau, F. Petroff, P. Etienne, G. Creuzet, A. Friederich, and J. Chazela, Phys. Rev. Lett. **61**, 2472 (1988); G. Binasch, P. Grünberg, F. Saurenbach, and W. Zinn, Phys. Rev. B **39**, 4828 (1989).

[3] S. Kaka, M. R. Pufall, W. H. Rippard, T. J. Silva, S. E. Russek, J. A. Katine, and M. Carry, J. Magn. Magn. Mater. **286**, 375 (2005); J. C. Sankey, P. M. Braganca, A. G. F. Garcia, I. N. Krivorotov, R. A. Buhrman, and D. C. Ralph, Phys. Rev. Lett. **96**, 227601 (2006); Q. Mistral, Joo Von Kim, T. Devolder, P. Crozat, C. Chappert, J. A. Katrine, M. J. Carey, and K. Ito, Appl. Phys. Lett. **88**, 192507 (2006).

[4] M. R. Pufall, W. H. Rippard, S. E. Russek, S. Kaka, T. J. Silva, and J. A. Katine, Phys. Rev. Lett. **97**, 087206 (2006).

[5] I. N. Krivorotov, N. C. Emley, J. C. Sankey, S. I. Kiselev, R. C. Ralph, and R. A. Burhman, Science **307**, 228 (2005); S. Kaka, M. R. Pufall, W. H. Rippard, T. J. Silva, S. E. Russek, and J. A. Katine, Nature (London) **437**, 389 (2005).

[6] For review, see M. D. Stiles and Jacques Miltat, in *Spin Dynamics in Confined Magnetic Structures III*, Topics in Applied Physics Vol. 101, edited by B. Hillebrands and A. Thiaville (Springer-Verlag, Heidelberg, 2006), p. 101.

[7] C. E. Zaspel, B. A. Ivanov, J. P. Park, and P. A. Crowell, Phys. Rev. B **72**, 024427 (2005); R. E. Arias and D. L. Mills, *ibid.* **72**, 104418 (2005).

[8] R. E. Arias and D. L. Mills, Phys. Rev. B **75**, 214404 (2007).

[9] T. M. Nguyen and M. G. Cottam, Phys. Rev. B **71**, 094406 (2005); T. M. Nguyen, M. G. Cottam, H. Y. Liu, Z. K. Wang, S. C. Ng, M. H. Kuok, D. J. Lockwood, K. Nielsch, and U. Gösele, *ibid.* **73**, 140402 (2006).

[10] R. Arias and D. L. Mills, Phys. Rev. B **63**, 134439 (2001).

[11] N. Smith, W. Doyle, D. Markham, and D. LaTourette, IEEE Trans. Magn. **23**, 3248 (1987).

[12] For a review, see B. Heinrich, J. F. Cochran, B. Hillebrands, G. Güntherodt, W. J. M. de Jonge, H. A. M. de Gronckel, and K. Kopinga, *Ultrathin Magnetic Structures: Measurement Techniques and Novel Magnetic Properties*, edited by B. Heinrich and J. A. C. Bland (Springer-Verlag, Berlin, 1994), Vol. 2, Chap. 3.

[13] R. P. Erickson and D. L. Mills, Phys. Rev. B **43**, 10715 (1991).

[14] R. W. Damon and J. R. Eshbach, J. Phys. Chem. Solids **19**, 308 (1961).

[15] W. F. Brown, *Micromagnetics* (Wiley, New York, 1963).

[16] W. H. Press, S. A. Teukolsky, W. T. Vetterling, and B. P. Flannery, *Numerical Recipes: The Art of Scientific Computing*, 3rd ed. (Cambridge University Press, New York, 2007), Vol. 1, pp. 964–977.

[17] The dynamical form of the free energy, analogous to Eq. (2), includes an exchange term whose variation results in a surface integral $\oint_S \hat{n}\cdot\nabla\hat{M}(\vec{x},t)\cdot\delta\hat{M}(\vec{x},t)d^2x_{\|}$, where $\hat{n}$ is outwardly normal to surface S. With $\delta\hat{M}(\vec{x},t)$ arbitrary, minimization requires $\partial\hat{M}(\vec{x},t)/\partial z|_{z=\pm z_0}=0$. Thus, the ground-state part of $\vec{M}(\vec{x},t) = M_0\hat{x}'(z) + \delta\vec{m}(\vec{x})\cdot\exp(-\Omega t)$ independently satisfies these conditions via $\dot{\theta}(\pm z_0)=0$, as in Eq. (3b), so it follows that the dynamical part satisfies these constraints via Eq. (12).

[18] See Ref. 16, pp 986–992, for further details.

[19] The diagonalization is that of a nonsymmetric matrix of dimension $2N-4$. Some years ago it was shown that a matrix of this form can always be diagonalized given the presence of a stable ground state. The result yields $N-2$ positive eigenvalues and $N-2$ negative eigenvalues, and each eigenvalue is associated with a pair of left and right eigenvectors. For further details, see R. P. Erickson and D. L. Mills, Phys. Rev. B **44**, 11825 (1991).

[20] See Ref. 12, pp 233–234.

[21] G. Bergmann, J. G. Lu, Y. Tao, and R. S. Thompson, Phys. Rev. B **77**, 054415 (2008).

[22] Pascal Lederer and D. L. Mills, Phys. Rev. **148**, 542 (1966); Y. B. Bazaliy, B. A. Jones, and Shou Chen Zhang, Phys. Rev. B **57**, R3213 (1998); J. Fernández-Rossier, M. Braun, A. S. Nuñez, and A. H. MacDonald, *ibid.* **69**, 174412 (2004).

[23] D. L. Mills and I. E. Dzyaloshinskii (unpublished).

[24] V. G. Bar'yakhtar, V. A. Lvov, and D. A. Yablonskii, JETP Lett. **37**, 673 (1983); M. Mostovoy, Phys. Rev. Lett. **96**, 067601 (2006); I. Dzyaloshinskii, Europhys. Lett. **83**, 67001 (2008).